Nucleation-vs-instability race in strained lms

Kailang Liu, Isabelle Berbezier, Thomas David, Luc Favre, Marco Abbarchi, Antoine Ronda, Peter Voorhees, Jean-Noël Aqua

Nucleation-vs-instability race in strained films

Kailang Liu,[†] Isabelle Berbezier,[†] Thomas David,[†] Luc Favre,[†] Marco Abbarchi,[†] Antoine Ronda,[†] Peter Voorhees,[‡] and Jean-Noël Aqua*,[¶]

[†]*Institut Matériaux Microélectronique Nanoscience de Provence, Aix-Marseille Université, UMR CNRS 6242, 13997 Marseille, France*
[‡]*Department of Materials Science and Engineering, Northwestern University, Evanston, Illinois 60208-3108*
[¶]*Institut des Nanosciences de Paris, Université Pierre et Marie Curie Paris 6 and CNRS UMR 7588, 4 place Jussieu, 75252 Paris, France*

E-mail: aqua@insp.jussieu.fr

Abstract

Under the generic term Stranski-Krastanov are grouped two different growth mechanisms of SiGe quantum dots. They result from a self-organized Asaro-Tiller-Grinfel'd (ATG) instability at low strain, while at high strain, from a stochastic nucleation. We elucidate here the puzzling difference between these two pathways thanks to a joint theoretical and experimental work. Nucleation is described within the master equation framework. By comparing the nucleation time scale and ATG characteristic time, we show that the former exhibits a strong exponential divergence at low strain while the latter behaves only algebraically. Consequently, at high/low strain, nucleation/instability occurs faster and inhibits the alternate evolution. The cross-over between the nucleation and ATG instability is found to occur both experimentally and theoretically at a Ge composition around 50%.

Keywords

self-organization, heteroepitaxy, quantum dots, instability, nucleation

Quantum dots are nowadays extensively grown by different techniques and used in a broad range of applications, from high-performance broadband photodiodes[1] to quantum information processing,[2] quantum cryptography with photon quantum bits (Qbits),[3,4] light emitting diodes with photonic QDs crystals in microcavity,[5] QDs transistors,[6] QDs solar cells,[7,8] etc. Many efforts have been devoted to circumvent the low quantum efficiency of Si and Ge QDs associated to indirect bandgap issue. Band folding in strained heterostructures was expected to create quasi-direct band structure[9–11] and to increase radiative recombination.[12] Various configurations of self-assembled Si/Ge multiple quantum dots(MQDs),[13] nanopatterned microdisks,[10] nanopatterned superlattices pyramidal QDs[14] have been elaborated to adjust the band structure.

Complex design of QDs devices allows to mix different signals such as spins and carriers or photons and carriers with a large variety of QDs per chip with multiple functions, whose placement and homogeneity commonly request a combination of nanotechnology and self-organization steps. Devices such as single (or some) electron transistors are also configured with one, two or three QDs closely packed on laterally confined active areas. Nevertheless, most QDs systems fabricated by nanotechnological tools are limited by their intrinsic lack of homogeneity, which reduces to only a small number of relevant dots to be achieved per chip. At the opposite, MOSFET devices require perfectly flat, Ge-rich, free of defects and fully strained 2D thin films epitaxially deposited on ultra-small transistor gate. Whatever the end-use application, ultimate fabrication of devices necessitates a perfect control of the island formation and evolution behavior over a large range of composition.

Despite the large number of studies dedicated to the SiGe system, an unified quantitative evolution of the QDs in different experimental conditions is still lacking. The outstanding challenge is to allow QDs control and scalability to engineer quantum devices based on QDs located at will. Since the QDs growth significantly differs in rather similar experiments and is a matter of confusion or controversy by a combination of theory and experiments we give here quantitative insights on the very first steps of this evolution.

In $Si_{1-x}Ge_x$ films on Si, one can taylor the amount of strain by varying the mean Ge concentration x. At low x, see Fig. 1, one finds an instability in connection with self-organized phenomena where dynamics builds long-range structures.[15,16] This instability is nucleationless[17,18] and leads after some coarsening to anisotropic quantum dots.[19] At high x conversely, see Fig. 1, the dots nucleate quickly and randomly without any long range order.[20,21] We develop here a kinetic model to rationalize the competition between the two mechanisms and to evaluate the cross-over concentration x_c that separates them. It incorporates the main ingredients that rule island growth, i.e. the driv-

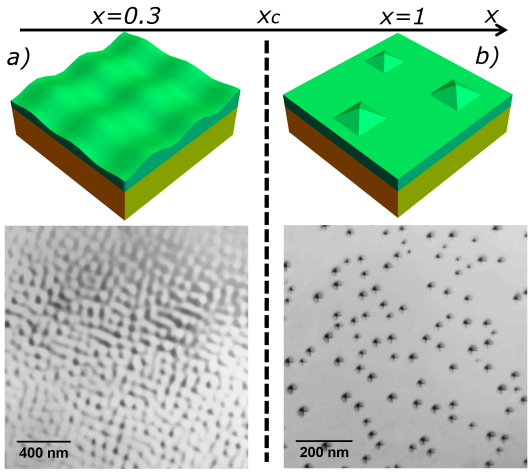

Figure 1: Graphical representation and TEM plane view images of the two growth modes at work in SiGe strained films ; a) at low strain for a typical $Si_{0.7}Ge_{0.3}$ film on Si(001) and b) at high strain for a typical Ge film on Si(001).

ing elasticity vs the inhibiting capillarity, and neglect other details such as reconstruction, alloying or inhomogeneities.[22] We derive an analytic expression for the dot energy as a function of its volume. The resulting energy barrier is found to noticeably depend on the amount of strain, i.e. on x, leading to a nucleation time scale that exponentially depends on $1/x$. Compared to the rather slow algebraic dependence of the ATG-instability characteristic time, we find a clear cross-over between the two time-scales. Using parameters of SiGe systems, we find a cross-over x_c typically around 0.5. This value is confirmed by experiments especially dedicated to investigating this cross-over.

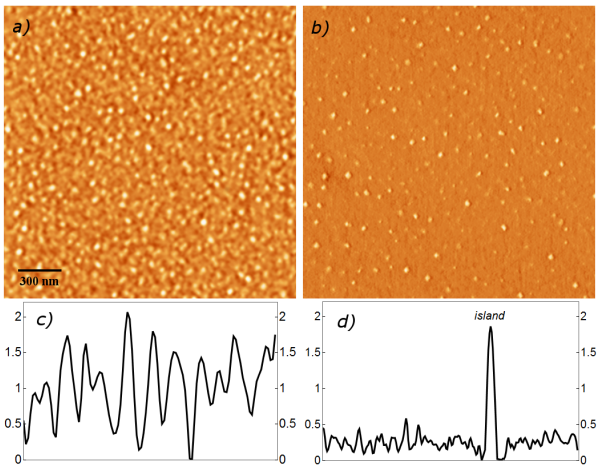

Figure 2: AFM images of (a) 2nm $Si_{0.5}Ge_{0.5}$ and (b) 1.3nm $Si_{0.4}Ge_{0.6}$ films deposited on Si(001). The image sizes are $2\mu m \times 2\mu m$ and their vertical scale is 7 nm. Images (c) and (d) are lines profiles corresponding respectively to (a) and (b).

The experiments to identify the two different evolution pathways are performed in a Riber MBE (Molecular-beam epitaxy) system with pressure down to 10^{-11} torr. The Si deposition flux is produced by electron-beam evaporation while the Ge flux comes from an effusion cell. The deposition rates are both precisely calibrated by reflection high-energy electron diffraction. The Si(001) substrate is firstly cleaned by chemical method and then transferred into the MBE growth chamber. After flashing the substrate at 1000 °C for 3 min, a buffer layer with a thickness of 40 nm is deposited to make a reproducible clean surface at 750 °C. Then, the substrate temperature is decreased to 550 °C, Si and Ge are co-deposited with SiGe rate of 0.04-0.05 nm/s. The sample holder is always kept rotating during the deposition. As deposition stops, the samples are immediately cooled down and subsequently taken out for morphological characterization using Atomic Force Microscopy in non-contact mode. We precisely control the epilayer thickness to catch the onset of surface roughening and thence the first steps of the morphological evolution. The two typical evolution pathways are clearly visible in Fig. 2 for a 2 nm thick $Si_{0.5}Ge_{0.5}$ film and for a 1.3 nm thick $Si_{0.4}Ge_{0.6}$ film.

In Fig. 2(a), the morphology roughens on the whole surface as described by the ATG instability.[17,18] The wavelength of this corrugation is conveniently extracted from a ring-like Fourier Transform image, in good agreement with the experimental results for this instability.[17] The continuous roughening is more clearly highlighted in a typical line profile in Fig. 2(c). On the contrary, for the $Si_{0.4}Ge_{0.6}$ film in Fig. 2(b), islands nucleate discretely on the surface while the rest of the substrate remains flat. This is evidenced by the profile in Fig. 2(d) that exhibits isolated islands separated by a wetting layer which roughness is around 0.3 nm, merely in the magnitude of AFM noise. Its Fourier Transform image is a full disk, showing no long-range order. As a consequence, we conclude that the cross-over concentration between the nucleation and instability growth mode lies in between 0.5 and 0.6 at 550 °C.

To characterize the nucleation process, we consider the classical theory of nucleation[23] which is adequate given the large critical sizes (a few hundreds of atoms) found in experiments.[24] We first compute the energy barrier associated with the formation of quantum dots[25–29] from a flat film, in the regime of homogeneous nucleation without considering the effect of atomic defects on the surface such as kinks or dimer vacancy lines.[30] For simplification, we assume that the islands have a square-base pyramidal shape with (105) facets that corresponds to the first well-defined hut clusters found in experiments after the initial pre-pyramid embryo.[24,31] This assumption allows to compute all the barriers analytically. The total energy results from the competition between elasticity and capillarity. The formation energy of the pyramid (the difference in energy between one pyramid of volume V on top of a wetting layer of thickness h_w, and one flat layer of thickness h_0)

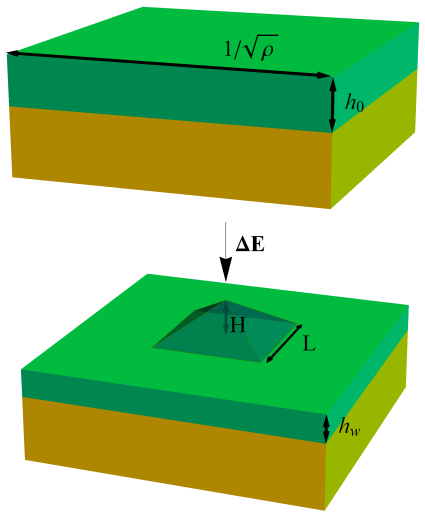

Figure 3: Geometry of the system, where each island with a square-base pyramidal geometry, grows on a "capture" zone $1/\rho$ on top of a wetting layer of thickness h_w.

is

$$\Delta E = \Delta E^{surf} + \Delta E^{ed} + \Delta E^{el}\,, \tag{1}$$

with the surface energy contribution ΔE^{surf}, the edge energy ΔE^{ed} and the elastic relaxation ΔE^{el}. Mass conservation enforces the balance $h_w = h_0 - \rho V/a$ where a is the lattice parameter ($a = 0.27$ nm in SiGe) and $1/\rho$, the surface available for each island.

The surface energies of the (001) and (105) facets, $\gamma^{(001)}$ and $\gamma^{(105)}$, depend on different parameters such as the film thickness, composition, etc. The surface composition of a SiGe film deposited on Si is still a matter of experimental investigation. One knows that Ge segregates so that the surface is enriched in Ge.[32] As a simplification, we consider the limiting case of a surface composition $x^s = 1$. It corresponds to experimental results that indicate a full enrichment of the surface in Ge even in deposited alloys.[33] Moreover, we consider films above their Stranski-Krastanov critical thickness so that wetting interactions do not enter significantly in the energy barrier. For a pyramid with facet angle θ, volume V and base length $L = \alpha V^{1/3}$ [with $\alpha = (6/\tan\theta)^{1/3}$], see Fig. 3, one finds

$$\Delta E^{surf} = \gamma_{Ge}^{(001)}\,\eta\,L^2\,, \tag{2}$$

with the capillary number

$$\eta = \frac{\gamma_{Ge}^{(105)}}{\gamma_{Ge}^{(001)}}\frac{1}{\cos\theta} - 1\,, \tag{3}$$

that describes the stability of the (001) surface with respect to faceting to (105). When $\eta > 0$, the creation of a (105) facet is overall a cost in energy, so that capillarity is a resistant force.[34,35] We consider in the following $\gamma_{Ge}^{(001)} = 60.5\,\mathrm{meV/\AA^2}$, see 36,37, while $\gamma_{Ge}^{(105)}$ is given by η as discussed below. Finally, we also include edge energy[25,28,38] to describe the pyramidal shape with a mean edge energy σ^{ed} for the pyramid and pyramid/wetting layer angles, so that

$$\Delta E^{ed} = \frac{4H}{\tan\theta}\left(2 + \sqrt{2 + \tan^2\theta}\right)\sigma^{ed}\,. \tag{4}$$

As regards elasticity, mechanical equilibrium equations may be solved exactly in the systems under investigation that display small slopes [at most 11° for the (105) facets]. In the small slope approximation, a film with a free surface $z = h(\boldsymbol{r})$ has an elastic energy[39]

$$\mathcal{E}^{el} = \mathcal{E}_0 \int d\boldsymbol{r}\,\{h(\boldsymbol{r}) - \zeta h(\boldsymbol{r})\mathcal{H}_{ii}[h(\boldsymbol{r})]\}\,, \tag{5}$$

with the energy density $\mathcal{E}_0 = Y_f m^2/(1-\nu_f)$ and coefficient $\zeta = Y_f(1-\nu_s^2)/Y_s(1-\nu_f)$, where Y and ν are the Young's modulus and Poisson's ratio while subscripts f and s refer to the film and substrate. The elastic contribution to the nucleation barrier can be computed exactly,[40] with the result

$$\Delta E^{el} = -\zeta\,p\,\mathcal{E}_0\,V\,, \tag{6}$$

for a square base pyramid, with

$$p = 4(\sqrt{2}-1)[1 + \ln(1+\sqrt{2})]\tan\theta/\pi\,. \tag{7}$$

As a whole, the energy barrier ΔE reduces to the typical form $\Delta E = \tilde{\sigma}v^{1/3} + \tilde{\gamma}v^{2/3} - \tilde{p}v$, with $\tilde{\sigma} = 2(2+\sqrt{2+\tan^2\theta})\sigma^{ed}$, $\tilde{\gamma} = \gamma_{Ge}^{(001)}\eta$, $\tilde{p} = \zeta\,p\,\mathcal{E}_0\tan\theta/6$ and $v = 6V/\tan\theta$. Its typical variation is plotted in Fig. 4 and shows the existence of an energy barrier ΔE^* at a critical volume V^* given by

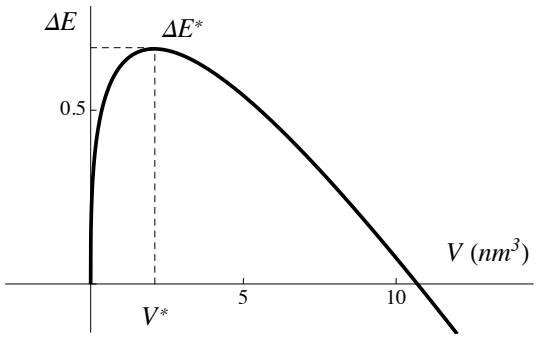

Figure 4: Nucleation barrier ΔE as a function of the pyramid volume V with the parameters described below.

$$\Delta E^* = \frac{1}{27\tilde{p}^2}\left[\tilde{\gamma}(2\,\tilde{\gamma}^2 + 9\,\tilde{p}\,\tilde{\sigma}) + 2(\tilde{\gamma}^2 + 3\,\tilde{p}\,\tilde{\sigma})^{3/2}\right]\,. \tag{8}$$

With this nucleation barrier, one can derive the nu-

cleation theory based on the master equation[23,41]

$$\frac{d\rho_n}{dt} = \sum_m \left[f_{m,n}\,\rho_m - f_{n,m}\,\rho_n \right] , \tag{9}$$

that relates the densities ρ_n of clusters with n atoms, with the frequencies $f_{m,n}$ of the transitions from m to n-atoms clusters. When only one-atom events occur, only the frequencies $f_n = f_{n,n+1}$ matter. They may be estimated as

$$f_n = \gamma_n\, \alpha D_s\, \rho_1 , \tag{10}$$

with the attachment coefficient γ_n, capture coefficient α, adatom density $\rho_1(t)$ and surface diffusion coefficient $D_s(T)$. In the following, we will use $\alpha \simeq 1$, $\gamma_n \simeq 1$, $D_s = a^2 \nu_0\, e^{-\beta E_{diff}}$ with $\nu_0 \simeq 10^{13}\,\mathrm{s}^{-1}$ and the diffusion barrier $E_{diff} = 0.83\,\mathrm{eV}$ in Si.[42] We also make the approximation $\rho_1 = \frac{1}{a^2} e^{-\beta E_2}$ with the attachment energy $E_2 \simeq 0.3\,\mathrm{eV}$. The master equation has a stationary solution characterized by a flux of nucleation per unit time and surface[23,41]

$$J^{st} = Z f_{n^*} \rho_{n^*} , \tag{11}$$

with f_{n^*}, the growth frequency of a critical cluster with n^* atoms (corresponding to the critical volume V^*), and the critical cluster density

$$\rho_{n^*} = \rho_1 e^{-\beta \Delta E^*} . \tag{12}$$

In (11), the Zeldovich factor is given by[23,41]

$$Z = \sqrt{ -\left. \frac{\partial^2 \Delta E}{\partial n^2} \right|_{n^*} \frac{1}{2\pi k_B T} } , \tag{13}$$

that reduces here to

$$Z = \frac{2a^3\sqrt{\beta}}{\tan\theta \sqrt{\pi \tilde{\sigma}^2}} \left(\tilde{\gamma} - \sqrt{\tilde{\gamma}^2 + 3\tilde{\sigma}\tilde{p}} \right) \left(\tilde{\gamma}^2 + 3\tilde{\sigma}\tilde{p} \right)^{1/4} . \tag{14}$$

The flux J^{st} is associated with the typical time scale for nucleation

$$\tau^{nuc} = \frac{1}{J^{st} \lambda^2} , \tag{15}$$

where we choose to consider nucleation over the typical island zone λ^2 defined by the experimental density $\lambda = 1/\sqrt{\rho}$, with $\rho \simeq 10^{13}\,\mathrm{m}^{-2}$.

With this time scale in hand, we turn to the ATG morphological instability.[43,44] It may be captured by the continuum description of surface diffusion governed by $\partial h/\partial t = D \Delta_s \mu$ with the diffusion coefficient D, surface Laplacian Δ_s and chemical potential μ.[42] The latter includes the capillary term $\gamma \Delta_s h$ and the elastic energy density $\mathcal{E}_0$ so that dimensional analysis leads to the instability space and time scales[45]

$$l_{ATG} = \frac{\gamma_f}{2\zeta \mathcal{E}_0} \quad \text{and} \quad t^{ATG} = \frac{l_{ATG}^4}{D\gamma_f} , \tag{16}$$

with the surface energy $\gamma_f = \gamma_{Ge}^{(001)}$ and the elastic energy density given above that is proportional to $m^2 = (0.042\,x)^2$. Hence, t^{ATG} is proportional to $1/x^8$.[‡‡] We plot in Figure 5 the typical time scales of the ATG instability and of nucleation. The nucleation time τ^{nuc} displays a strong exponential increase at low x, overshooting the rather slow varying t^{ATG}. Hence, we argue

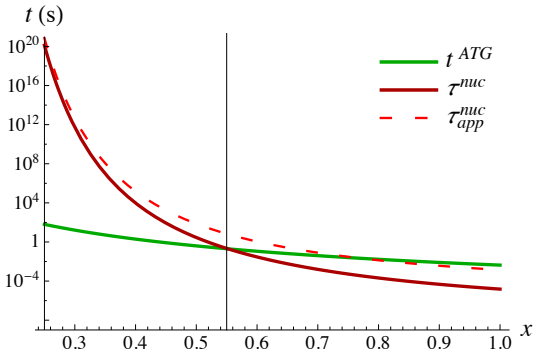

Figure 5: Typical time scales for nucleation τ^{nuc} (red–dark grey line) and ATG instability t^{ATG} (green–light grey line) as a function of the film Ge composition x for $\eta = 0.003$ and $\sigma^{ed} = 3.3\,\mathrm{meV/\AA}$. The red dotted line corresponds to the analytic approximation (17).

that the two pathways (instability vs nucleation) are dictated by kinetics: for large enough x, $\tau^{nuc} \ll t^{ATG}$ so that nucleation occurs first, relaxes partially the elastic strain and prevents the occurrence of the ATG instability. On the contrary, for low enough x, $\tau^{nuc} \gg t^{ATG}$ and only the instability has time to occur.

The cross-over between the two time scales may be rationalized by the strong decrease in the critical clusters density ρ_{n^*} when x decreases. Indeed, when x decreases, the surface energy contribution is constant while the amplitude of the elastic relaxation decreases as $\mathcal{E}_0 \propto x^2$ so that the maximum for ΔE, ΔE^*, increases. Because this energy barrier enters in a Boltzmann factor in ρ_{n^*}, the nucleation rate exponentially decreases with x. To quantify this effect, one may simplify the expression of J^{st} by performing a small-x expansion of ΔE^*, with the result

$$\tau^{nuc} \approx \tau_0^{nuc}\, e^{\beta \left(b \frac{\gamma^3}{x^4} + c \frac{\gamma \sigma^{ed}}{x^2} \right)} , \tag{17}$$

with some constants τ_0^{nuc}, b and c. This approximation is shown in Fig. 5 and does indeed match the exact result at low x. With this approximation, it is clear that the capillary-vs-elasticity balance leads to a strong $\exp(1/x^4)$ divergence of τ^{nuc} at low-x that quickly overshoots the ATG time scale that 'only' behaves as $1/x^8$. The system under study may include extra effects such as: alloying (intermixing, segregation, surface inhomogeneities), surface reconstruction inhomogeneity and evolution, wetting effects, surface stress, inhomogeneous nucleation etc. However, we argue that the main scenario ruling the cross-over between the ATG instability

[‡‡] we use in the following $D = \beta D_0\, c\, \Omega$, with the vacancy surface concentration $c \simeq 1/a^2$, $\Omega = a^3$ and $D_0 = 8.45\,10^{-10} e^{-\beta E_d}\,\mathrm{m^2 s^{-1}}$ with $E_d = 0.83\,\mathrm{eV}$[42]

and nucleation is contained in this scenario: when x decreases, the elastic driving force decreases, the energy barrier increases so that nucleation occurs over an exponentially divergent time scale.

The data in Fig. 5 are computed with parameters typical of SiGe systems as described above [‡‡]. The intersection between the two time-scales occurs around $x_c \simeq 0.55$ that is consistent with the experimental results but that is dependent on the model parameters as described below. The classical nucleation theory includes different parameters that are only approximate (capture zone, etc) but which precise values are not relevant for the existence of the cross-over. The two parameters that prove to be quantitatively important for x_c are the capillary number η and edge energy σ^{ed}. We consider here a positive but small capillary number $\eta = 0.003$ that corresponds to $\gamma_{Ge}^{(105)} = 59.5\,\mathrm{meV/Å^2}$, only 1 meV lower than $\gamma_{Ge}^{(001)}$. This value leads to a cross-over x_c in the vicinity of 0.55 for $\sigma^{ed} = 3.3\,\mathrm{meV/Å}$. The latter edge energy is lower but comparable with the atomistic estimation in Ref. 46 that is 10 meV/Å. Given the different uncertainties of the model, the comparison between theory and experiment is satisfactory.

To go further, we characterize the parameter dependence of the model. The more crucial parameters are η and σ^{ed}. For σ^{ed} =3 and 4 meV/Å, one finds $x_c = 0.50$ and 0.71 respectively for $\eta = 0.003$. Also, for $\eta = 0.0046$ and 0.0013 (that correspond to $\gamma_{Ge}^{(001)} = 59.4$ and $59.6\,\mathrm{meV/Å^2}$), one finds $x_c = 0.73$ and 0.37 for σ^{ed} =3.3 meV/Å. Furthermore, by changing the temperature to $T = 650°\mathrm{C}$, we get $x_c \simeq 0.48$. At higher temperatures, intermixing is supposed to play a significant role[19] and will decrease the elastic driving force. The surface composition proves also to be important. By changing x_s to 0.9, we find $x_c = 0.8$ using a Vegard's law for the surface energy with $\gamma_{Si} = 90\,\mathrm{meV/Å^2}$ both for (001) and (105) orientations[36,37]–note that in this case η changes significantly to 0.0053. We also changed the geometric pathway by computing numerically the elastic energy for a truncated pyramid that typically leads to an decrease in ΔE^* of 0.1 eV. As a conclusion, given the uncertainties in the different parameters (surface concentration, reconstruction, alloying ...), the choice of parameters here is plausible and validates the overall scenario with a cross-over expected to be around 0.5.

As a conclusion, we performed a joint experimental and theoretical work to rationalize the competition between two growth modes in strained films : the nucleation of islands and the ATG morphological instability, that both eventually lead to quantum dots. We show experimentally in SiGe systems that the instability occurs for a Ge concentration $x \lesssim 0.5$ while quantum dots stochastically nucleate at higher $x \gtrsim 0.6$. We computed the nucleation barrier and time scale τ^{nuc} from rate theory. We show that τ^{nuc} diverges exponentially at low x, with a Boltzmann factor $\exp[\alpha/k_B T x^4]$ while the instability time scale evolves only as $1/x^8$. Consequently, the competition between the nucleation and instability pathways is ruled by kinetics : nucleation occurs at large strain but is frozen at small strain, allowing time for the instability to occur. Additional effects such as alloying[47] or patterning[48] could be investigated in future work, e.g. using kinetic Monte-Carlo simulations.[49]

Acknowledgement Kailang Liu thanks CSC for financial support

[‡‡] As regards elasticity, $\nu^{Si} = 0.279$, $\nu^{Ge} = 0.273$, $Y^{Si} = 1.30\,10^{11}\,\mathrm{J/m^3}$, $Y^{Ge} = 1.03\,\mathrm{J/m^3}$, $a = 0.27\,\mathrm{nm}$

1, The silicon attachment energy (0.3eV) comes from which reference?
2, The last comment of Peter in the discussion seems not so clear.
3, The heterogeneous nucleation mentioned in the very beginning of modeling introduction

References

(1) Michel, J.; Liu, J.; Kimerling, L. C. *Nature Photonics* **2010**, *4*, 527–534.

(2) Juska, G.; Dimastrodonato, V.; Mereni, L. O.; Gocalinska, A.; Pelucchi, E. *Nature Photonics* **2013**, *7*, 527–531.

(3) O'Brien, J. L.; Pryde, G. J.; White, A. G.; Ralph, T. C.; Branning, D. *Nature* **2003**, *426*, 264–267.

(4) Bayer, M.; Hawrylak, P.; Hinzer, K.; Fafard, S.; Korkusinski, M.; Wasilewski, Z.; Stern, O.; Forchel, A. *Science* **2001**, *291*, 451–453.

(5) Xia, J.; Ikegami, Y.; Shiraki, Y.; Usami, N.; Nakata, Y. *Applied physics letters* **2006**, *89*, 201102.

(6) Biasotto, C.; Nanver, L.; Moers, J.; Gerharz, J.; Mussler, G.; van der Cingel, J.; Zhang, J.; Bauer, G.; Schmidt, O.; Miglio, L. *IEEE electron device letters* **2010**, *31*, 1083–1085.

(7) Tayagaki, T.; Hoshi, Y.; Usami, N. *Scientific reports* **2013**, *3*.

(8) Luque, A.; Martí, A. *Physical Review Letters* **1997**, *78*, 5014.

(9) Zabel, T.; Sircar, N.; Hauke, N.; Zweck, J.; Döblinger, M.; Kaniber, M.; Finley, J. J.; Abstreiter, G.; Arakawa, Y.; Bougeard, D. *Applied Physics Letters* **2013**, *103*, 063105.

(10) Chen, R.; Gupta, S.; Huang, Y.-C.; Huo, Y.; Rudy, C. W.; Sanchez, E.; Kim, Y.; Kamins, T. I.; Saraswat, K. C.; Harris, J. S. *Nano letters* **2013**, *14*, 37–43.

(11) Jain, J. R.; Hryciw, A.; Baer, T. M.; Miller, D. A.; Brongersma, M. L.; Howe, R. T. *Nature Photonics* **2012**, *6*, 398–405.

(12) Barbagiovanni, E.; Lockwood, D.; Rowell, N.; Costa Filho, R.; Berbezier, I.; Amiard, G.; Favre, L.; Ronda, A.; Faustini, M.; Grosso, D. *Journal of Applied Physics* **2014**, *115*, 044311.

(13) Yakimov, A.; Kirienko, V.; Armbrister, V.; Bloshkin, A.; Dvurechenskii, A. *Physical Review B* **2014**, *90*, 035430.

(14) Pinto, S. R.; Buljan, M.; Chahboun, A.; Roldan, M.; Bernstorff, S.; Varela, M.; Pennycook, S.; Barradas, N.; Alves, E.; et.al, *Journal of Applied Physics* **2012**, *111*, 074316.

(15) Pidduck, A. J.; Robbins, D. J.; Cullis, A. G.; Leong, W. Y.; Pitt, A. M. *Thin Solid Films* **1992**, **222**, 78.

(16) Berbezier, I.; Gallas, B.; Ronda, A.; Derrien, J. *Surf. Sci.* **1998**, **412**, 415.

(17) Sutter, P.; Lagally, M. G. *Phys. Rev. Lett.* **2000**, **84**, 4637.

(18) Tromp, R. M.; Ross, F. M.; Reuter, M. C. *Phys. Rev. Lett.* **2000**, **84**, 4641.

(19) Aqua, J.-N.; Berbezier, I.; Favre, L.; Frisch, T.; Ronda, A. *Phys. Rep.* **2013**, **522**, 59.

(20) Eaglesham, D. J.; Cerullo, M. *Phys. Rev. Lett.* **1990**, *64*, 1943.

(21) Mo, Y. W.; Savage, D. E.; Swartzentruber, B. S.; Lagally, M. G. *Phys. Rev. Lett.* **1990**, *65*, 1020.

(22) Villain, J. *J. Cryst. Growth* **2005**, **275**, e2307.

(23) Kashchiev, D. *Nucleation, basic theory with application*; Butterworth-Heinemann, 2000.

(24) Voigtänder, B. *Surf. Sci. Rep.* **2001**, **43**, 127.

(25) Shchukin, V. A.; Ledentsov, N. N.; Kop'ev, P. S.; Bimberg, D. *Phys. Rev. Lett.* **1995**, *75*, 2968.

(26) Müller, P.; Kern, R. *Appl. Surf. Sci.* **1996**, *102*, 6.

(27) McKay, M. R.; Venables, J. A.; Drucker, J. *Phys. Rev. Lett.* **2008**, *101*, 216104.

(28) Brehm, M.; Montalenti, F.; Grydlik, M.; Vastola, G.; Lichtenberger, H.; Hrauda, N.; Beck, M. J.; Fromherz, T.; Schäffler, F.; Miglio, L.; Bauer, G. *Phys. Rev. B* **2009**, *80*, 205321.

(29) Li, X. L.; Wang, C. X.; Yang, G. W. *Progress Mater. Sc.* **2014**, **64**, 121.

(30) F. Liu, F.; Wu, F.; Lagally, M. G. *Chem. Rev.* **1997**, *97*, 1045.

(31) (a) Vailionis, A.; Cho, B.; Glass, G.; Desjardins, P.; Cahill, D. G.; Greene, J. E. *Phys. Rev. Lett* **2000**, *85*, 3672; (b) Szkutnik, P. D.; Sgarlata, A.; Nufris, S.; Motta, N.; Balzarotti, A. *Physical Review B* **2004**, *69*, 201309–.

(32) (a) Nakagawa, K.; Miyao, M. *J. Appl. Phys.* **1991**, **69**, 3058; (b) Liu, F.; Lagally, M. G. *Phys. Rev. Lett.* **1996**, *76*, 3156; (c) Voigtländer, B.; Kästner, M. *Phys. Rev. B* **1999**, *60*, R5121; (d) Capellini, G.; De Seta, M.; Evangelisti, F. *Appl. Phys. Lett.* **2001**, *78*, 303; (e) Leite, M. S.; Gray, J. L.; Hull, R.; Floro, J. A.; Magalhães Paniago, R.; Medeiros-Ribeiro, G. *Phys. Rev. B* **2006**, *73*, 121308; (f) Brehm, M.; Grydlik, M.; Lichtenberger, H.; Fromherz, T.; Hrauda, N.; Jantsch, W.; Schäffler, F.; Bauer, G. *Applied Physics Letters* **2008**, *93*, 121901.

(33) (a) Portavoce, A.; Bassani, F.; Ronda, A.; Berbezier, I. *Surf. Sci.* **2002**, *519*, 185; (b) Berbezier, I.; Descoins, M.; Ismail, B.; Maaref, H.; Ronda, A. *J. Appl. Phys.* **2005**, **98**, 063517.

(34) Daruka, I.; Grossauer, C.; Springholz, G.; Tersoff, J. *Phys. Rev. B* **2014**, *89*, 235427.

(35) Contrarily, $\eta < 0$ would describe a system where the creation of (105) is a driving force. It was put forward to rationalize the existence of nanowires in sub-critical systems, see Chen, G. and Sanduijav *et al*, *Phys. Rev. Lett.* **2012** *108* 055503, but entropic effects, reconstruction coexistence and composition inhomogeneities enforce a high level of uncertainty.

(36) Lu, G.-H.; Liu, F. *Phys. Rev. Lett.* **2005**, **94**, 176103.

(37) Scopece, D.; Montalenti, F.; Beck, M. J. *Physical Review B* **2012**, *85*, 085312–.

(38) Lozovoy, K. A.; Kokhanenko, A. P.; Voitsekhovskii, A. V. *Cryst. Growth Des.* **2015**, *15*, 1055.

(39) Aqua, J.-N.; Frisch, T. *Phys. Rev. B* **2010**, **82**, 085322.

(40) Duport, C.; Priester, C.; Villain, J. In *Equilibrium shape of a coherent epitaxial cluster*; Zhang, Z., Lagally, M. G., Eds.; World Scientific, Singapore, 1997; p 73.

(41) Ratke, L.; Voorhees, P. W. *Growth and coarsening*; Springer, 2010.

(42) Spencer, B. J.; Voorhees, P. W.; Davis, S. H. *Phys. Rev. Lett.* **1991**, **67**, 3696.

(43) Asaro, R. J.; Tiller, W. A. *Metall. Trans.* **1972**, **3**, 1789.

(44) Grinfeld, M. A. *Sov. Phys. Dokl.* **1986**, **31**, 831.

(45) (a) Aqua, J.-N.; Gouyé, A.; Ronda, A.; Frisch, T.; Berbezier, I. *Phys. Rev. Lett.* **2013**, **110**, 096101; (b) Aqua, J.-N.; Gouyé, A.; Auphan, T.; Frisch, T.; Ronda, A.; Berbezier, I. *Appl. Phys. Lett.* **2011**, **98**, 161909.

(46) Retford, C. M.; Asta, M.; Miksis, M. J.; Voorhees, P. W.; Webb, E. B. *Phys. Rev. B* **2007**, *75*, 075311.

(47) Bergamaschini, R.; Tersoff, J.; Tu, Y.; Zhang, J. J.; Bauer, G.; Montalenti, F. *Phys. Rev. Lett.* **2012**, *109*, 156101.

(48) (a) Hu, H.; Gao, H. J.; Liu, F. *Phys. Rev. Lett.* **2008**, *101*, 216102; (b) Xu, X.; Aqua, J.-N.; Frisch, T. *J. Phys. : Condens. Matter* **2012**, *24*, 045002.

(49) (a) Lam, C.-H.; Lee, C.-K.; Sander, L. M. *Phys. Rev. Lett.* **2002**, *89*, 216102; (b) Gaillard, P.; Aqua, J.-N.; Frisch, T. *Phys. Rev. B* **2013**, *87*, 125310.

Graphical TOC Entry